Applied Physics A (2020) 126:568
https://doi.org/10.1007/s00339-020-03740-x

Applied Physics A
Materials Science & Processing

Analysis of shape memory alloy vibrator using harmonic balance method

Haoyuan Du[1] · Xuan He[1] · Linxiang Wang[1] · Roderick Melnik[2]

Received: 9 April 2020 / Accepted: 19 June 2020 / Published online: 29 June 2020

Abstract
Shape memory alloy (SMA) is a very important smart material, which has been widely used in many fields, especially in vibration. Phase transformation can be induced by changing temperature and its stiffness changes accordingly. In this paper, the primary resonance vibration of a one-dimensional SMA oscillator is analyzed using the harmonic balance (HB) method. The amplitude-frequency curves of the SMA oscillator with different temperatures are drawn, and the effect of temperature and frequency on the amplitude is discussed. Then, the energy flow of SMA in the vibration process is researched by the power flow analysis (PFA) approach. The time-averaged input power (TAIP) is calculated using the analytical and numerical method, respectively, and the calculation time is compared. It is found that the difference between the analytical and numerical solutions is not significant in most cases, but the calculation time of analytical solution is only about one-tenth of that of the numerical solution, which is very important in saving computational cost, real-time control and so on. Finally, some other characteristics of energy flow in the SMA oscillator are identified.

Keywords Shape memory alloy · Analytical solution · Amplitude–frequency characteristics · Power flow analysis

1 Introduction

Due to the important and unique thermo-mechanical properties, shape memory alloys (SMA) are widely known and used. It can convert thermal energy into mechanical energy directly, and vice versa [1], which makes it very attractive in many engineering applications, such as mechanical engineering, biomedicine, robotics and so on [2–8]. Among the applications mentioned above, SMA vibration damper may be the most common one [1, 9]. When the temperature changes, the phase transformation between the martensite phase (at low temperature) and the austenite phase (at high temperature) can be induced in SMA materials [10–12]. And at low temperatures, SMA material can be switched between multiple martensitic variants by external loading [13]. These phenomena can be explained by the theory of Landau theory of phase transition, and the potential energy of a typical SMA with different temperatures is plotted as Fig. 1 [10, 13].

As shown in Fig. 1, when the temperature is relatively low, as curve a, there are only two local minima in the potential energy diagram of SMA, which represents the twin martensite phase with different orientations. When no external load is applied, only the two martensite phases are stable due to the minimum potential energy. However, when the external force applied to SMA is large enough, the energy barrier will be overcome and martensite will change from the original phase to another. When the temperature rises as shown in curve b, both martensite and austenite will exist, and the minimum in the middle is the austenite phase, while the minima on both sides correspond to the twin martensite phase. The twin martensite phase stable for it corresponds to the lowest potential energy, while the austenite phase corresponds to a metastable state. In addition, when the temperature is further increased as curve c, the austenite phase stable for it corresponds to the lowest potential energy, while the twin martensite phase corresponds to a metastable state. When the external load is removed, SMA will return to the martensite state, which generates the pseudoelasticity [10]. Moreover, when the temperature is high enough as curved,

✉ Linxiang Wang
wanglx236@zju.edu.cn

[1] State Key Laboratory of Fluid Power and Mechatronic Systems, Zhejiang University, 310027 Hangzhou, People's Republic of China

[2] MS2Dicovery Interdisciplinary Research Institute, Wilfrid Laurier University, Waterloo, ON N2L 3L5, Canada

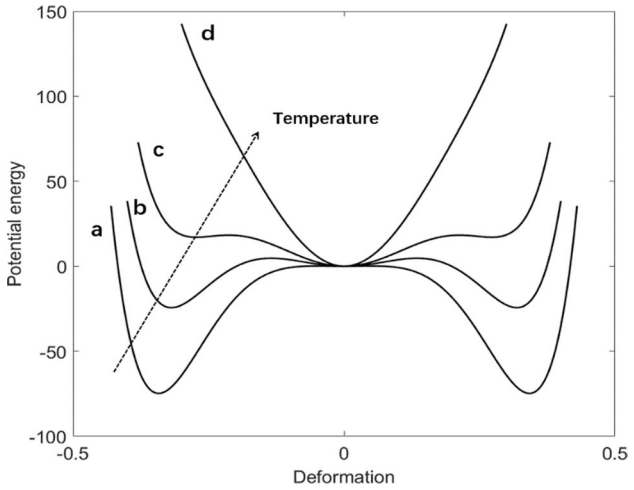

Fig. 1 Sketch of the potential energy of a typical SMA with different temperatures

there is only one minimum in the whole potential energy curve. At this time, the twin martensite phase has disappeared and only austenite is stable and exists.

When traditional mass-spring damped oscillators are used to absorb vibration, the frequency of excitation is usually required to be known or close to the natural frequency of the target system [13]. But in practical application, the frequency of the target system is often unknown in advance [14]. Therefore, the oscillator with adjustable stiffness is very important and at the same time, the frequency of the oscillator can be adjusted according to the change of the target frequency. It is found that the introduction of non-linear elements can make the system possess many advantages that linear systems do not possess [13, 15, 16]. For example, Oueini et al. [15] found that the effective working frequency of the linear counterparts could be enlarged by the nonlinear vibration absorbers. By introducing a nonlinear negative stiffness mechanism, the vibration isolators perform better in the low-frequency range compared with linear ones [16]. The unique characteristics of SMA enable them to have large stiffness at high temperatures (in the austenite phase) and softer at low temperatures (in the martensite phase). Its stiffness could be changed correspondingly with the change of temperature. Therefore, it is feasible to achieve this goal using the mechanical–thermal coupling property of shape memory alloy [13, 17–19]. The effect of pressure on thermal and structural transitions in the SMAs was researched by Canbay et al. [11]. It was found that the martensitic transformation could be influenced by the order–disorder transition. And the activation energy of the SMA sample was calculated using Kissinger method. Wang et al. [13] researched the application of the SMA in tuning structural vibration frequencies using numerical methods and it was demonstrated that using the SMA oscillator, the frequency of the system can be adjusted in a wide range. However, the existing literature mainly uses the numerical method to analyze the characteristics of SMA. Although the numerical solution is a generalized method for solving various systems with periodic/quasi-periodic or even chaotic motions, it is computationally expensive [20]. In contrast, the approximate solutions using the harmonic balance method are less computational cost and have more physical insight.

The vibration power flow analysis (PFA) approach is a common method to analyze dynamic systems and complex structures [20]. Compared with traditional single force or velocity, vibration power flow provides more accurate performance indicators of vibration level [21]. A power flow mode theory was developed by Xiong et al. [22] and the dynamic system inherent power flow behavior was revealed. The vibration control requirements could be satisfied using the proposed energy flow design approaches. Moreover, the power flow analysis approach was also used to assess the energy harvesting efficiency of a nonlinear blade system [23]. Besides, the power flow of nonlinear isolation systems and the effectiveness of nonlinear isolators from the perspective of vibration power flow were analyzed in Refs. [16] and [24]. However, the study of energy flow in the SMA oscillator is very limited.

In this paper, the damped oscillator of a one-dimensional SMA oscillator is researched. The first-order harmonic balance method is applied to analyze the primary resonance occurred in the system. The amplitude–frequency characteristic curves of shape memory alloy are calculated, and the effect of different temperature and load frequency on the amplitude is researched. In addition, the time-averaged input power (TAIP) and maximum kinetic energy in the SMA oscillator are analyzed using the PFA approach. The super-harmonic resonance, sub-harmonic resonance, bifurcation and chaos phenomena appearing in the vibration of SMA oscillators are all worth trying with analytical solutions, but they cannot be realized by the first-order harmonic balance method. These phenomena will be discussed in future articles using a high-order harmonic balance method or multi-scale method, etc.

2 Analysis of amplitude–frequency response

A typical one-dimensional damped vibration system consisting of an SMA rod is shown in Fig. 2. The restoring force of the SMA rod is as follows [13]:

$$F_s = k_1(\theta - \theta_0)x + k_2x^3 + k_3x^5, \tag{1}$$

where k_1, k_2, k_3 are material-special constants and θ_0 is the reference transformation temperature. The restoring force can be tuned by changing the temperature θ.

The damping of the system is as follows:

$$f_c = c\dot{x}. \tag{2}$$

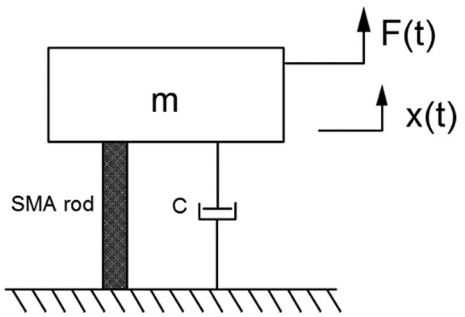

Fig. 2 Sketch of the 1-D SMA damped vibration system

The input force is assumed as a sinusoidal function

$$F(t) = A_0 \cos(\omega t), \tag{3}$$

where A_0 is the amplitude of the force.

The parameters of this system are got from the Ref. [13] as $m = 5$ kg, $c = 100$Ns/m, $\theta_0 = 208$ K, $k_1 = 459.6$ kg/s^2 K, $k_2 = -3.59 \times 10^5$ kg/s^2 m^2, $k_3 = 3 \times 10^6$ kg/s^2 m^4, $A_0 = 2000$ N. The length of the shape memory alloy rod is chosen as $L = 4$ m and the area is 3.83×10^{-5} m^2.

The relationship between the force and deformation with four temperatures is plotted according to Eq. (1) to demonstrate the temperature influence on the stiffness of the SMA rod.

As can be seen from the Fig. 3a, when the temperature is 210 K, the relationship between the applied external force and the deformation is non-linear. The curve AC section is unstable, and there will be a hysteresis phenomenon. The curve will jump directly from A to B or from C to D [13, 25, 26] and the input energy will be dissipated. When the temperature rises to 230 K, the phase transition of martensite and austenite exists combined with Fig. 1 curve c. However, at 230 K, the energy barrier between austenite and martensite is smaller than that of twin martensite at 210 K, which means that hysteresis is easier to induce in this case. Similar to that at 210 K, curve AC is still unstable and the hysteretic phenomenon exists as shown in Fig. 3b. When the temperature rises to 320 K and 400 K, only austenite phase exists, so there is no phase transformation and hysteresis. The relationship between deformation and the external force is close to linear, and the higher the temperature, the closer it is.

According to Newton's second law, the governing equation for the system is as follows:

$$m\ddot{x} + c\dot{x} + k_1(\theta - \theta_0)x + k_2x^3 + k_3x^5 = A_0 \cos(\omega t). \tag{4}$$

Equation (4) is further simplified as

$$\ddot{x} + 2\xi\dot{x} + \alpha(\theta - \theta_0)x + \beta x^3 + \gamma x^5 = f \cos(\omega t). \tag{5}$$

To get analytical approximations of the system solution, the harmonic balance (HB) method is used for this system exhibiting periodic solutions. The solution can be expanded into Fourier series:

$$x = x_0 + \sum_{n=1}^{N} \left(a_n \cos\left(n\omega_0 t\right) + b_n \sin\left(n\omega_0 t\right)\right), \tag{6a}$$

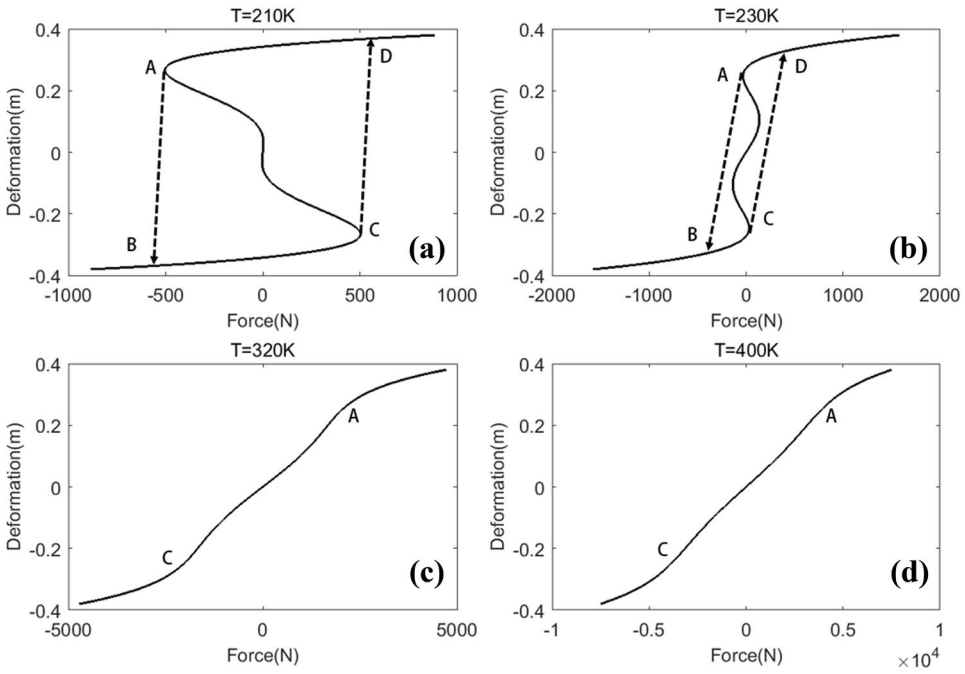

Fig. 3 The deformation-force relations of the SMA rod. **a** $\theta = 220$ K, **b** $\theta = 260$ K, **c** $\theta = 320$ K, **d** $\theta = 400$ K

$$\dot{x} = \omega \sum_{n=1}^{N} \left(-na_n \sin\left(n\omega_0 t\right) + nb_n \cos\left(n\omega_0 t\right)\right), \tag{6b}$$

$$\ddot{x} = \omega^2 \sum_{n=1}^{N} \left(-n^2 a_n \cos\left(n\omega_0 t\right) - n^2 b_n \sin\left(n\omega_0 t\right)\right). \tag{6c}$$

It is reasonable to assume that the solution has the same frequency as the input force and for simplicity, the first-order approximation is used for the solution:

$$x = x_0 + a_1 \cos(\omega t) + b_1 \sin(\omega t). \tag{7}$$

Since the average amplitude of the input force is 0, it can be inferred that $x_0 = 0$, thus the solution can be written as

$$x = a_1 \cos(\omega t) + b_1 \sin(\omega t). \tag{8}$$

Then, the first and second derivatives of the solution are:

$$\dot{x} = -a_1 \omega \sin(\omega t) + b_1 \omega \cos(\omega t), \tag{9a}$$

$$\ddot{x} = -a_1 \omega^2 \cos(\omega t) - b_1 \omega^2 \sin(\omega t). \tag{9b}$$

Fourier series expansion for x^3 and x^5 is calculated as

$$x^3 = \frac{3}{4}\left[a_1\left(a_1^2 + b_1^2\right)\cos(\omega t) + b_1\left(a_1^2 + b_1^2\right)\sin(\omega t)\right], \tag{10a}$$

$$x^5 = \frac{5}{8}\left[a_1\left(a_1^2 + b_1^2\right)^2 \cos(\omega t) + b_1\left(a_1^2 + b_1^2\right)^2 \sin(\omega t)\right]. \tag{10b}$$

Substitute the above into the governing equation, and make the coefficients corresponding to the left and right sides of the $\cos(\omega t)$ and $\sin(\omega t)$ equal:

$$\begin{aligned} &-a_1\omega^2 + 2b_1\xi\omega + a_1\left(\theta - \theta_0\right)\alpha \\ &+ \frac{3}{4}a_1\left(a_1^2 + b_1^2\right)\beta + \frac{5}{8}a_1\left(a_1^2 + b_1^2\right)^2\gamma = f, \end{aligned} \tag{11a}$$

$$\begin{aligned} &-b_1\omega^2 - 2a_1\xi\omega + b_1\left(\theta - \theta_0\right)\alpha \\ &+ \frac{3}{4}b_1\left(a_1^2 + b_1^2\right)\beta + \frac{5}{8}b_1\left(a_1^2 + b_1^2\right)^2\gamma = 0. \end{aligned} \tag{11b}$$

The coefficient a_1 and b_1 are solved as follows:

$$a_1 = \frac{f\left(-\omega^2 + \alpha\left(\theta - \theta_0\right) + \frac{3}{4}\beta X^2 + \frac{5}{8}\gamma X^4\right)}{\left(-\omega^2 + \alpha\left(\theta - \theta_0\right) + \frac{3}{4}\beta X^2 + \frac{5}{8}\gamma X^4\right)^2 + (2\xi\omega)^2}, \tag{12a}$$

$$b_1 = \frac{2f\xi\omega}{\left(-\omega^2 + \alpha\left(\theta - \theta_0\right) + \frac{3}{4}\beta X^2 + \frac{5}{8}\gamma X^4\right)^2 + (2\xi\omega)^2}, \tag{12b}$$

in which X is the amplitude of the oscillation and can be calculated as

$$X = \left(a_1^2 + b_1^2\right)^{1/2}. \tag{13}$$

Combined with Eqs. (12) and (13), the relationship of the oscillation amplitude (X) and angular frequency (ω) of the input stress is calculated as

$$X^2 = \frac{f^2}{\left(-\omega^2 + \alpha\left(\theta - \theta_0\right) + \frac{3}{4}\beta X^2 + \frac{5}{8}\gamma X^4\right)^2 + (2\xi\omega)^2}. \tag{14}$$

Using Eq. (14), the amplitude–frequency curves of the SMA damping system with the temperature (θ) of 220 K, 260 K, 320 K, and 400 K are plotted in Fig. 4. It is shown that when the temperature is 220 K as shown in Fig. 4a, there are two or three amplitude values that are plotted as orange and yellow corresponding one angular frequency when it is about 20–50 rad/s. Thus, it is unstable and the leap phenomenon will occur which is a peculiar phenomenon of non-linear systems. When the frequency sweeps from left to right, the curve follows the path of A–B–D and when the frequency sweeps from right to left, the curve follows the path of D–C–A.

When the temperature is higher as 260 K as shown in Fig. 4b, the non-linear relationship between force and deformation is weaker than that at 220 K, so the amplitude–frequency curve is relatively close to the linear system. But the skeleton curve is still slightly skewed like other non-linear systems. When the temperature is 320 K and 400 K, respectively, as shown in Fig. 3, there is an approximately linear relationship between force and deformation. Thus, the corresponding amplitude–frequency curves are similar to the linear system which has only one peak and as the temperature increases, the resonance frequency becomes higher.

To better analyze the vibration of the SMA oscillator, the amplitude is taken as a function of temperature (θ) and angular frequency (ω), and the 3D curve of temperature-angular frequency–amplitude is drawn in Fig. 5,in which the angular frequency and temperature are 1–1000 rad/s and 210–400 K, respectively. For ease of observation, the 3D curve is shown from two different perspectives. In this curve, it can be seen that when the temperature is low, two or three stress amplitudes are corresponding to the same angular frequency. The multi-solutions are marked in green and blue. These are unstable and the leap phenomenon will occur like Fig. 4a, the specific value of the amplitude depends on the frequency variation trend. Besides, with the increase of temperature, the amplitude–frequency curve tends to be similar to the linear system, and the resonance frequency increases gradually, while the amplitude decreases.

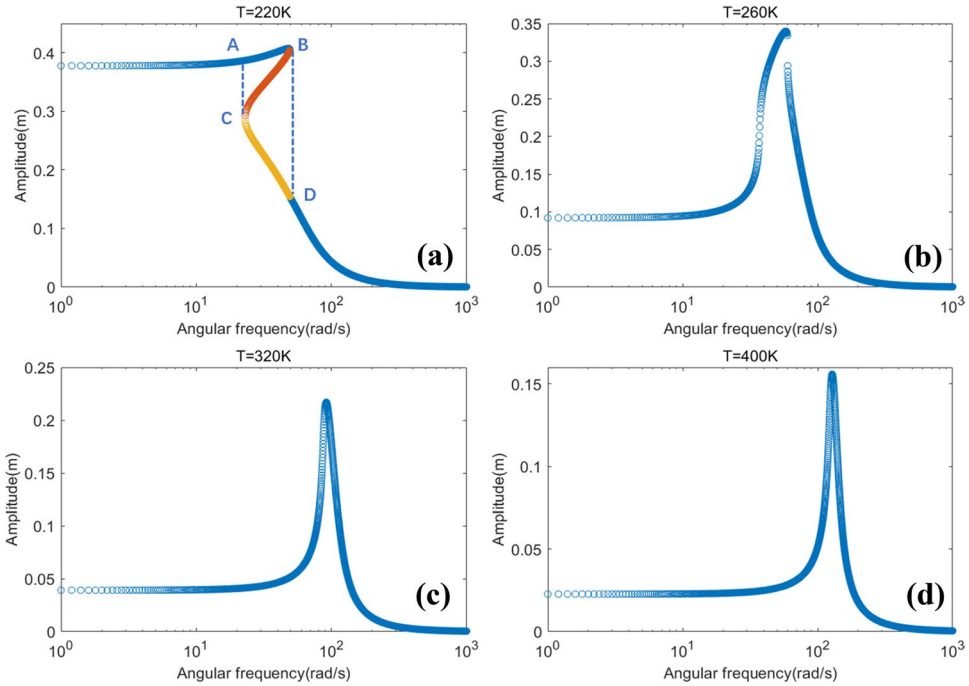

Fig. 4 The amplitude-frequency curves of the SMA rod. **a** $\theta = 220$ K, **b** $\theta = 260$ K, **c** $\theta = 320$ K, **d** $\theta = 400$ K

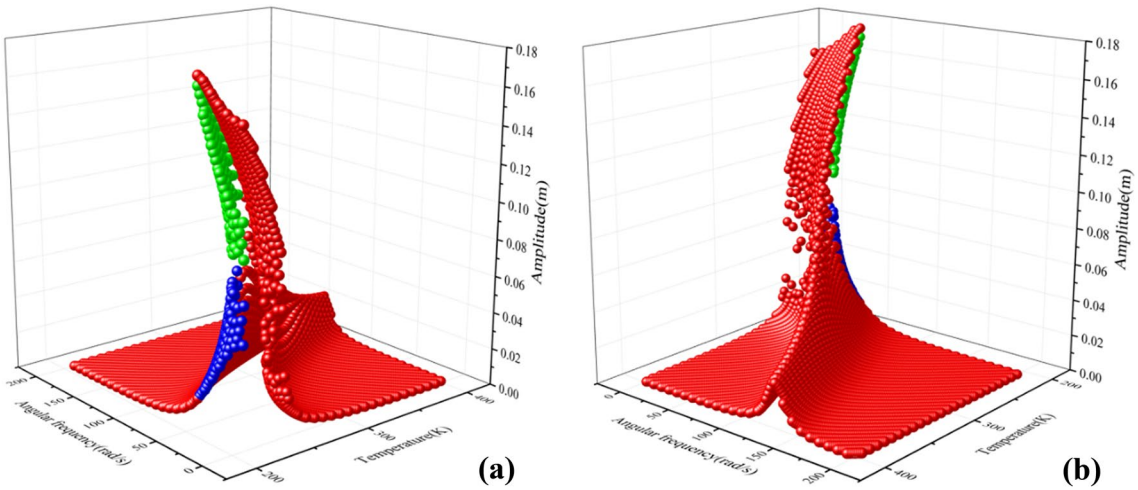

Fig. 5 The amplitude–frequency 3-D curve of the SMA rod with the angular frequency $1 - 1000$ rad/s and temperature $210 - 400$ K

3 Power flow analysis of the system

3.1 Formulations

The velocity $\dot{x}$ of the mass is multiplied on both sides of the Eq. (5) and the power flow balance equation can be obtained [20]:

$$\dot{K} + \dot{U} + P_{\mathrm{d}} = P_{\mathrm{in}}, \tag{15}$$

where $\dot{K}$,$\dot{U}$, P_{d} and P_{in} are time change rates of the kinetic energy, potential energy, dissipated and input power, respectively. Their expressions are as follows:

$$\dot{K} = \ddot{x}\dot{x}, \tag{16a}$$

$$\dot{U} = \alpha\left(\theta - \theta_0\right)\dot{x}x + \beta\dot{x}x^3 + \gamma\dot{x}x^5, \tag{16b}$$

$$P_{\mathrm{d}} = 2\xi\dot{x}^2, \tag{16c}$$

$$P_{\mathrm{in}} = \dot{x}f\cos\left(\omega t\right). \tag{16d}$$

Integration over time is made for Eq. (15) from t_{i} to $t_{\mathrm{i}} + t_{\mathrm{p}}$, and the displacement at $t = t_{\mathrm{i}}$ and $t = t_{\mathrm{i}} + t_{\mathrm{p}}$ are x_{i} and x, respectively. The equation can be obtained as follows:

$$\Delta K + \Delta U + E_{\mathrm{d}} = E_{\mathrm{in}}, \tag{17}$$

where

$$\Delta K = \frac{\dot{x}^2 - \dot{x}_{\mathrm{i}}^2}{2}, \tag{18a}$$

$$\begin{aligned}\Delta U &= \int_{t_{\mathrm{i}}}^{t_{\mathrm{i}}+t_{\mathrm{p}}} \left(\alpha\left(\theta - \theta_0\right)\dot{x}x + \beta\dot{x}x^3 + \gamma\dot{x}x^5\right)\mathrm{d}t \\ &= \frac{\alpha\left(\theta - \theta_0\right)\left(x^2 - x_{\mathrm{i}}^2\right)}{2} + \frac{\beta\left(x^4 - x_{\mathrm{i}}^4\right)}{4} + \frac{\gamma\left(x^6 - x_{\mathrm{i}}^6\right)}{6},\end{aligned} \tag{18b}$$

$$E_{\mathrm{d}} = \int_{t_{\mathrm{i}}}^{t_{\mathrm{i}}+t_{\mathrm{p}}} 2\xi\dot{x}^2\mathrm{d}t, \tag{18c}$$

$$E_{\mathrm{in}} = \int_{t_{\mathrm{i}}}^{t_{\mathrm{i}}+t_{\mathrm{p}}} \dot{x}f\cos\left(\omega t\right)\mathrm{d}t, \tag{18d}$$

respectively, represent the kinetic and potential energy and total dissipated and input energy changes.

Thus, the time-averaged dissipated and input energy are formulated, respectively, as

$$\overline{P}_{\mathrm{d}} = \frac{E_{\mathrm{d}}}{t_{\mathrm{p}}} = \frac{1}{t_{\mathrm{p}}}\int_{t_{\mathrm{i}}}^{t_{\mathrm{i}}+t_{\mathrm{p}}} 2\xi\dot{x}^2\mathrm{d}t, \tag{19a}$$

$$\overline{P}_{\mathrm{in}} = \frac{E_{\mathrm{in}}}{t_{\mathrm{p}}} = \frac{1}{t_p}\int_{t_{\mathrm{i}}}^{t_{\mathrm{i}}+t_{\mathrm{p}}} \dot{x}f\cos\left(\omega t\right)\mathrm{d}t. \tag{19b}$$

3.2 Solving methods

The analytical solutions of instantaneous input power can be written as follows using Eqs. (6b) and (16d):

$$\begin{aligned}P_{\mathrm{in}} = \frac{f\omega}{2}\sum_{n=1}^{N} n\{-a_n\left[\sin\left(n\omega_0 + \omega\right)t + \sin\left(n\omega_0 - \omega\right)t\right] \\ + b_n\left[\cos\left(n\omega_0 + \omega\right)t + \cos\left(n\omega_0 - \omega\right)t\right]\}.\end{aligned} \tag{20}$$

It is obvious that over a period, only the stationary part with $n\omega_0 - \omega = 0$ of the P_{in} can give a non-zero value and the TAIP can be formulated as

$$\overline{P}_{\mathrm{in}} = \frac{1}{2}f\omega_0 n b_n, \tag{21}$$

where $n = \omega/\omega_0$.

3.3 Power flow behavior

3.3.1 Basic characteristics of the TAIP

The first-order approximation is also adopted in the analysis of the power flow and the n in Eq. (21) is adopted as 1. Some manipulations of Eq. (12) can lead to

$$\left[-\omega^2 + \alpha\left(\theta - \theta_0\right)\right]X^2 + \frac{3}{4}\beta X^4 + \frac{5}{8}\gamma X^6 = fa_1, \tag{22a}$$

$$2\xi\omega X^2 = fb_1. \tag{22b}$$

Based on the above formulations, several conclusions about the energy flow of this system can be made

$$\left\{\left[-\omega^2 + \alpha\left(\theta - \theta_0\right)\right]X + \frac{3}{4}\beta X^3 + \frac{5}{8}\gamma X^5\right\}^2 + \left(2\xi\omega X\right)^2 = f^2. \tag{23}$$

According to (21) and (22b), the TAIP over one period can be formulated as

$$\overline{P}_{\mathrm{in}} = \xi X^2\omega^2. \tag{24}$$

According to the auxiliary angle formula, the maximum velocity of the mass is

$$\dot{x}_{\max} = \omega\left(a_1^2 + b_1^2\right)^{1/2} = \omega X, \tag{25}$$

which corresponds to the maximum kinetic energy $K_{\max}$

$$K_{\max} = \frac{1}{2}X^2\omega^2. \tag{26}$$

Using Eqs. (24) and (26), the relation between TAIP and the maximum velocity can be seen:

$$\overline{P}_{\text{in}} = 2\xi K_{\max}. \tag{27}$$

Thus, the $\overline{P}_{\text{in}}$ is proportional to the maximum kinetic energy $K_{\max}$ and the proportional coefficient is the quotient of damping (c) and mass (m).

Using the Eqs. (14), (24) and (26), the TAIP over one period can be written as

$$\overline{P}_{\text{in}} = \frac{\xi f^2}{\frac{\left\{\left[-\omega^2+\alpha(\theta-\theta_0)\right]+\frac{3}{4}\beta X^2+\frac{5}{8}\gamma X^4\right\}^2}{\omega^2}+4\xi^2}, \tag{28}$$

and the maximum kinetic energy is

$$K_{\max} = \frac{1}{2}\frac{f^2}{\frac{\left[-\omega^2+\alpha(\theta-\theta_0)+\frac{3}{4}\beta X^2+\frac{5}{8}\gamma X^4\right]^2}{\omega^2}+4\xi^2}. \tag{29}$$

Then, the TAIP of the system using Eq. (28) with a temperature of 220 K, 260 K, 320 K and 400 K, and angular frequency 1–1000 rad/s is calculated and plotted in Fig. 6. The default dB reference for $\overline{P}_{\text{in}}$ and $K_{\max}$ is set as 10^{-12}. Meanwhile, the numerical solutions of the system can be obtained by transforming Eq. (5) into two first-order differential equations and solving it using a Runge–Kutta method and then make the numerical integration of Eq. (19b). Both analytical and numerical solutions are drawn in Fig. 5 where the red circle represents the analytic solution and the black solid line represents the numerical solution. It can be seen from the Fig. 6 that the analytical solution at 220 K is not well-fitted with the numerical solution at low-frequency band mainly because of subharmonic oscillation and only the first-order approximation is used, but it is almost the same as the numerical solution at high frequency and other temperatures.

In addition, the calculation time of the analytical solution and numerical solution using the software *Matlab* at different temperatures are recorded. The average time of the analytical solution is 21.0 s, while the average time of the numerical solution is 211.2 s. Therefore, the use of an analytical solution is more efficient and faster, which has great advantages for real-time control and so on.

3.3.2 Other characteristics

Combining Eqs. (28) and (29), the TAIP and maximum kinetic energy have upper bounds:

$$\overline{P}_{\text{in}} \le \frac{f^2}{4\xi} = \overline{P}_{\max}, \tag{30a}$$

$$K_{\max} \le \frac{f^2}{8\xi^2}. \tag{30b}$$

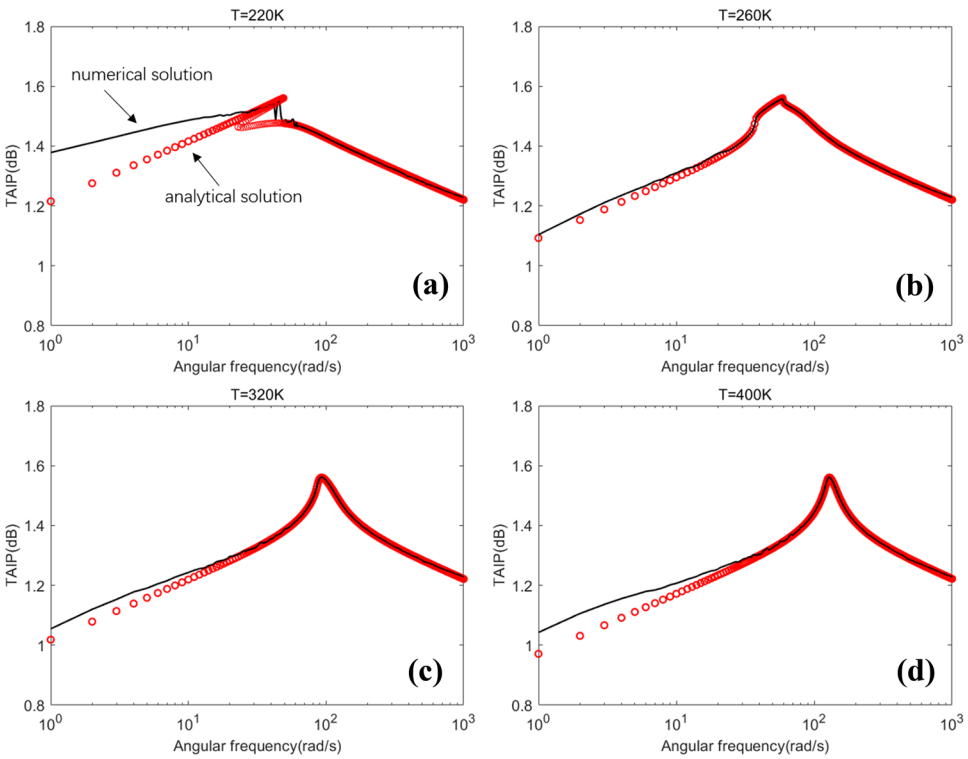

Fig. 6 The analytical and numerical solutions of the TAIP curves of the SMA rod. **a** $\theta = 220$ K, **b** $\theta = 260$ K, **c** $\theta = 320$ K, **d** $\theta = 400$ K

It can be seen that the maximum of $\overline{P}_{in}$ and $K_{\max}$ only depends on the amplitude of the excitation force and the damping coefficient. When the equation

$$\left[-\omega^2+\alpha\left(\theta-\theta_0\right)\right]+\frac{3}{4}\beta X^2+\frac{5}{8}\gamma X^4=0, \tag{31}$$

is satisfied, the upper bound can be reached and combing with Eq. (14), the equation about X^2 can be obtained:

$$\frac{5}{8}\gamma X^6+\frac{3}{4}\beta X^4+\alpha\left(\theta-\theta_0\right)X^2-\frac{f^2}{4\xi^2}=0. \tag{32}$$

Considering Eq. (32) as a cubic equation of X^2 and using Sheng Jin's Distinguishing Means [27] to study the characteristics of its solutions.The simplest multiple root discriminant of the equation is

$$A=\frac{9}{16}\beta^2-\frac{15}{8}\alpha\gamma\left(\theta-\theta_0\right), \tag{33a}$$

$$B=\frac{3}{4}\alpha\beta\left(\theta-\theta_0\right)+\frac{45}{32}\frac{\gamma f^2}{\xi^2}, \tag{33b}$$

$$C=\left[\alpha\left(\theta-\theta_0\right)\right]^2+\frac{9}{16}\frac{f^2\beta}{\xi^2}. \tag{33c}$$

The total discriminant of the equation is

$$\Delta=B^2-4AC. \tag{34}$$

When A and B are both 0, the equation has a triple real root; When $\Delta<0$, the equation has three different real roots; When Δ equals 0, the equation three real roots, two of which has the same value; When Δ is larger than 0, the equation has a real number root and a pair of conjugate imaginary roots [27].

It can be seen from Eq. (33) that coefficients A,B and C are mainly determined by temperature θ. When the value of temperature makes Δ fit in one of first three cases, the maximum TAIP can be achieved. Therefore, it can be seen temperature has a great influence on SMA, the behavior of the SMA vibrator can be manipulated by changing the temperature.

Moreover, when the frequency of the excitation is relatively high, the TAIP and the maximum kinetic energy approach to a fixed value, respectively:

$$\overline{P}_{\text{in}}=\frac{\xi f^2}{\omega^2+4\xi^2}, \tag{35}$$

$$K_{\max}=\frac{1}{2}\frac{f^2}{\omega^2+4\xi^2}. \tag{36}$$

According to the above equations, it can be seen that the stiffness parameters (k_1, k_2 and k_3) of the SMA do not have much influence on the oscillator under high-frequency working condition, which can provide reference for the SMA vibrator analysis at high frequency.

4 Conclusion

In this paper, the one-dimensional shape memory alloy oscillator is analyzed. The first-order harmonic balance (HB) method is used to analyze the primary resonance that occurred in the system. The amplitude–frequency curves of the SMA oscillator at different temperatures are plotted. It is found that when the temperature is relatively low, there will be an unstable region due to the transformation of twin martensite phases; thus, there will be a leap phenomenon. When the temperature rises, the unstable region disappears. But the skeleton curve is still slightly skewed, which is very similar to other non-linear vibration. Besides, the 3D curve of temperature-angular frequency–amplitude is drawn to have a better analysis of the SMA vibrator. It is found that with the increasing of temperature, the resonance frequency increases gradually, while the amplitude decreases. When the temperature is high enough, the curve is very similar to that of a linear system.

Moreover, according to the power flow analysis (PFA) approach, the power flow in the vibration of the SMA oscillator is analyzed. The time-averaged input power (TAIP) is calculated using the analytical and numerical method (Runge–Kutta method), respectively, for comparison. It is found that there is a slight difference between the analytical solution and numerical solution in most cases, but the calculation time of analytical solution is only about one-tenth of that of the numerical solution, which is very important in saving computational cost, real-time control and so on. Some other characteristics of the energy flow in the SMA oscillator are also discussed. It is found that the temperature has a great influence on SMA, the maximum of the TAIP and maximum kinetic energy can be achieved by changing the temperature. Finally, it is shown that the stiffness parameters of the SMA do not have much influence on the TAIP and the maximum kinetic energy of the vibrator under high-frequency working condition.

Acknowledgments This work was supported by the National Natural Science Foundation of China (Grant No. 51575478 and Grant No. 61571007).

References

1. L.X. Wang, R.V.N. Melnik, Numerical model for vibration damping resulting from the first-order phase transformations. Appl. Math. Model. **31**(9), 2008–2018 (2007)
2. Q. Wang, X.U. Zhiwei, Q. Zhu, Structural design of morphing trailing edge actuated by SMA. Front. Mech. Eng. **8**(3), 268–275 (2013)
3. G. Borchert, C. Lochte, G. Carbone et al., A modular design kit for task-adaptable low-cost robots based on BaPaMan design. Front. Mech. Eng. **8**(1), 33–41 (2013)
4. P.B.C. Leal, M.A. Savi, D.J. Hartl, Aero-structural optimization of shape memory alloy-based wing morphing via a class/shape transformation approach. Proc. Inst. Mech. Eng. Part G: J. Aerosp. Eng. **232**(15), 2745–2759 (2018)
5. M.H. Moghadam, M.R. Zakerzadeh, M. Ayati, Development of a cascade position control system for an SMA-actuated rotary actuator with improved experimental tracking results. J. Braz. Soc. Mech. Sci. Eng. **41**(10), 407 (2019)
6. Y. Zhishan, L. Dezhi, C. Yue, F. Zhaowei, L. Juntao, S. Zaiyan, Z. Ming, X. Xiaodong, W. Xingquan, Grikin Advanced Materials Co. Ltd, Research progress on the phase transformation behavior, microstructure and property of NiTi based high temperature shape memory alloys. Rare Metal Mater. Eng. **47**(7), 2269–2274 (2018)
7. X. Wang, S. Kustov, J. Van Humbeeck, A short review on the microstructure, transformation behavior and functional properties of NiTi shape memory alloys fabricated by selective laser melting. Materials **11**(9), 1683 (2018)
8. C.A. Canbay, A. Tataroğlu, W.A. Farooq, A. Dere, A. Karabulut, M. Atif et al., CuAlMnV shape memory alloy thin film based photosensitive diode. Mater. Sci. Semicond. Process. **107**, 104858 (2020)
9. G. Song, N. Ma, H.N. Li, Application of shape memory alloys in civil structures. Eng. Struct. **28**, 1266–1274 (2006)
10. X. He, Z. Tong, H. Du et al., Modeling microstructure evolution in shape memory alloy rods via Legendre wavelets collocation method. J. Mater. Sci. **54**(23), 14400–14413 (2019)
11. C.A. Canbay, T. Polat, Thermal and structural alternations in CuAlMnNi shape memory alloy by the effect of different pressure applications. Phys. B Phys. Condens. Matter **521**, 331–338 (2017)
12. C.A. Canbay et al., Investigation of thermoelastical martensitic transformations and structure in new composition of CuAlMnTi shape memory alloy. J. Mater. Electron. Dev. **1**(1), 60–64 (2019)
13. L. Wang, R.V.N. Melnik, Nonlinear dynamics of shape memory alloy oscillators in tuning structural vibration frequencies. Mechatronics **22**(8), 1085–1096 (2012)
14. G.L. McGavin, G. Guerin, Real-time seismic damping and frequency control of steel structures using Nitinol wire. Proc SPIE **4696**, 176–184 (2002)
15. S.S. Oueini, A.H. Nayfeh, J.R. Pratt, A nonlinear vibration absorber for flexible structures. Nonlinear Dyn. **15**(3), 259–282 (1998)
16. J. Yang, Y.P. Xiong, J.T. Xing, Dynamics and power flow behavior of a nonlinear vibration isolation system with a negative stiffness mechanism. J. Sound Vib. **332**(1), 167–183 (2013)
17. A. Masuda, M. Noori, Optimisation of hysteretic characteristics of damping devices based on pseudoelastic shape memory alloys. Int. J. Nonlinear Mech. **37**, 1375–1386 (2002)
18. E. Rustighi, M.J. Brennan, B.R. Mace, A shape memory alloy adaptive tuned vibration absorber: design and implementation. Smart Mater. Struct. **14**, 19–28 (2005)
19. S. Saadat, J. Salichs, M. Noori, Z. Hou, H. Davoodi, I. Bar-on et al., An overview of vibration and seismic applications of NiTi shape memory alloy. Smart Mater. Struct. **11**, 218–229 (2002)
20. J. Yang, Y.P. Xiong, J.T. Xing, Nonlinear power flow analysis of the Duffing oscillator. Mech. Syst. Signal Process **45**(2), 563–578 (2014)
21. H.G.D. Goyder, R.G. White, Vibrational power flow from machines into built-up structures. J. Sound Vib. **68**(1), 59–117 (1980)
22. Y.P. Xiong, J.T. Xing, W.G. Price, A power flow mode theory based on a system's damping distribution and power flow design approach. Proc. R. Soc. A: Math. Phys. Eng. Sci. **461**(2063), 3381–3411 (2005)
23. J. Yang, Y.P. Xiong, J.T. Xing, Investigations on a nonlinear energy harvesting device consisting of a flapping foil and an electro-magnetic generator using power flow analysis, in *23th Biennial Conference on Mechanical Vibration and Noise, ASME IDETC/CIE Conferences, Washington, DC, USA, August 29–21, Washington* (2011), pp. 1–8
24. J. Yang, Y.P. Xiong, J.T. Xing, Examinations of nonlinear isolators using power flow approach. in *23rd International Congress of Theoretical and Applied Mechanics (ICTAM2012), International Union of Theoretical and Applied Mechanics (IUTAM), Beijing, China, August 19–24, Beijing* (2012), pp. 1–2
25. N. Bubner, Landau-Ginzburg model for a deformation-driven experiment on shape memory alloys. Continu Mech. Therm. **8**(5), 293–308 (1996)
26. L.X. Wang, R.V.N. Melnik, Thermo-mechanical wave propagation in shape memory alloy rod with phase transformations. Mech. Adv. Mater. Struct. **14**(8), 665–676 (2007)
27. S. Fan, A new extracting formula and a new distinguishing means on the one variable cubic equation. Nat. Sci. J. Hainan Teach. Coll. **2**(2), 91–98 (1989)